UCSF

UC San Francisco Previously Published Works

Authors

Charafeddine, Rabab A
Cortopassi, Wilian A
Lak, Parnian
et al.

Peer reviewed

Conserved tau microtubule-binding repeat histidines confer pH-dependent tau-microtubule association

Rabab A. Charafeddine[1], Wilian A. Cortopassi[2], Parnian Lak[2], Ruensern Tan[3], Richard J. McKenney[3], Matthew P. Jacobson[2], Diane L. Barber[1], and Torsten Wittmann[1]

[1]Department of Cell & Tissue Biology, University of California, San Francisco,
[2]Department of Pharmaceutical Chemistry, University of California, San Francisco
[3]Department of Molecular and Cellular Biology, University of California, Davis

Running title: *pH-modulated tau-microtubule binding*

To whom correspondence should be addressed: torsten.wittmann@ucsf.edu, Department of Cell & Tissue Biology, University of California, San Francisco, 513 Parnassus Avenue; San Francisco, CA 94143-0512, USA, Tel.: (415) 476 2603

ABSTRACT

Tau, a member of the MAP2/tau family of microtubule-associated proteins, functions to stabilize and organize axonal microtubules in healthy neurons. In contrast, tau dissociates from microtubules and forms neurotoxic extracellular aggregates in neurodegenerative tauopathies. MAP2/tau family proteins are characterized by three to five conserved, intrinsically disordered repeat regions that mediate electrostatic interactions with the microtubule surface. We use molecular dynamics, microtubule-binding experiments and live cell microscopy to show that highly conserved histidine residues near the C terminus of each MT-binding repeat are pH sensors that can modulate tau-MT interaction strength within the physiological intracellular pH range. At lower pH, these histidines are positively charged and interact with phenylalanine residues in a hydrophobic cleft between adjacent tubulin dimers. At higher pH, tau deprotonation decreases microtubule-binding both in vitro and in cells. However, electrostatic and hydrophobic characteristics of histidine are required for tau-MT-binding as substitution with constitutively positively charged, non-aromatic lysine or uncharged alanine greatly reduces or abolishes tau-MT binding. Consistent with these findings, tau-MT binding is reduced in a cancer cell model with increased intracellular pH but is rapidly rescued by decreasing pH to normal levels. Thus, these data add a new dimension to the intracellular regulation of tau activity and could be relevant in normal and pathological conditions.

Neuronal development and function rely on a class of structural microtubule (MT)-associated proteins (MAPs) that share conserved MT-binding motifs. These MAP2/tau family proteins associate with MTs in an extended conformation along the MT protofilament ridge (1, 2), and binding is thought to be mediated largely through electrostatic interactions of basic amino acids distributed throughout the MAP2/tau family MT-binding repeats with the negatively charged MT wall. Tau (MAPT), the most intensely studied member of the MAP2/tau family, is expressed in both the developing and adult nervous system, and different tau splice variants contain either three or

four MT-binding repeats (3). In adult neurons, tau-MT binding is restricted to the axon. Tau is thought to influence MT stability and mechanics and to regulate axonal transport potentially by organizing inter-MT spacing in the axonal MT bundle (4–6), but its physiological function and regulation is still poorly understood.

Tau is also a key player in progressive neurodegenerative diseases, such as Alzheimer's disease and frontotemporal dementia. These and other tauopathies are characterized by a loss of axonal tau-MT association and an abnormal extracellular accumulation of aggregated tau (7, 8) although it remains controversial if these tau neurofibrillary tangles are a cause or consequence of neurodegeneration. Both the spatial control of tau-MT binding in normal neurons and the pathological dissociation from MTs highlight the importance of understanding how tau-MT-binding is controlled. Tau has many phosphorylation sites and as is the case with other MT-binding proteins, tau phosphorylation decreases its affinity for MTs, and pathological tau aggregates are formed by all splice variants of hyperphosphorylated tau (8, 9).

However, the intracellular environment is complex and many incompletely understood factors contribute to the control of protein interactions and functions (10). One such underappreciated regulator is intracellular pH (pH_i) (11). In contrast to previous static views of pH_i homeostasis, we now know that pH_i is dynamic and changes, for example, during cell cycle progression (12, 13), cell adhesion (14, 15), and migration (16–18). In addition, dysregulated pH_i is a feature of many diseases, including cancer (19, 20) and neurodegenerative disorders (21, 22). Although protein pH sensitivity is generally mediated by histidines with a pK_a near neutral, other titratable residues can also play critical roles depending on the protein energy landscape and cooperativity (11). Consequently, several examples have emerged in which histidine protonation dynamics regulate protein-protein (23, 24), protein-nucleotide (25), and protein phospholipid interactions (26, 27). Because all MAP2/tau family MT-binding repeats contain invariant histidine residues, we used *in silico*, *in vitro* and *in vivo* methods to ask if tau-MT binding is sensitive to changes in pH_i. Consistent with the modulation of electrostatic interactions, we find that tau-MT-binding is decreased at increased pH,

which opens new directions for understanding tau-MT binding dynamics in normal and pathological cell behaviours.

RESULTS

Conserved histidine residues contribute to tau-MT interactions

Recent cryo-electron microscopy (cryo-EM) data of MT-bound tau at near atomic resolution (28) indicate that tau-MT interactions extend beyond the central KxGS MT-binding repeat motif. In particular, the structure of the second tau MT-binding repeat (R2) shows that a highly conserved histidine residue, His299, near the R2 C-terminus may contribute to tau-MT binding. His299 points into a hydrophobic cleft defined by β-tubulin Phe399 and Phe395 near the interdimer interface, and His299 is in a T-shaped configuration with Phe399 (Fig. 1C).

Because of the negative electrostatic potential of the MT surface (Fig. 1A), the pK_a of His299 is estimated to be upshifted to about 7.0 when compared with the imidazole group in solution that has a pK_a of 6.3 (29). A positively charged $His299^+$ imidazolium cation is further stabilized by favorable electrostatic interactions with negatively charged β-tubulin Glu442 and is within reach of other hydrophobic contacts (< 7 Å) with β-tubulin residues near the inter-tubulin dimer cleft (Fig. 1C). Based on this analysis, we predicted that His299 is positively charged at neutral pH. His299 protonation could thus be regulated through changes in pH that fall within the physiological range. In contrast, solvent-exposed lysine and arginine residues in the MT-binding repeats have pK_a values >10 and are always protonated near neutral pH values. We therefore asked how positively charged $His299^+$ or neutral $His299^0$ could affect the interaction between tau R2 and MTs by *in silico* molecular dynamics (MD).

Based on the cryo-EM structure, we built models of the tau R2-MT complex with different His299 protonation states. Both systems were then evaluated in short time MD simulations (5 ns). In the model containing positively charged $His299^+$, the T-shaped interaction with Phe399 was maintained throughout the entire simulation (Fig. 1C; supplementary Video S1), with distances not exceeding 5 Å and in agreement with the cryo-EM structure. In contrast, neutral $His299^0$ turned away

from the hydrophobic cleft and remained in this position during the MD simulation. This also caused higher deviation from the tau-MT cryo-EM structure (RMSD = 2.9 Å) when compared with $His299^+$ (RMSD = 1.9 Å) as well as globally increased conformational fluctuations in both tubulin and tau (supplementary Fig. S1). Although our simulations analyzed only the one of the 3-4 tau MT-binding repeats for which a cryo-EM structure was available, the MT-binding repeat histidine residues in positions equivalent to His299 are highly conserved (Fig. 1D) (1, 2). In addition, 3R and 4R tau isoforms bind MTs in a similar manner utilizing the full length of the respective MT-binding repeat region (30). Because individually weak MT-binding repeats act together to support high affinity tau-MT interactions (31), histidine deprotonation at increased pH in multiple repeats may thus cooperatively weaken the tau-MT interaction and consequently destabilize the tau-MT complex.

Increased pH decreases tau-MT binding

To test the hypothesis that increased pH weakens tau-MT binding, we first used an *in vitro* MT co-sedimentation assay. The standard PIPES buffer used in such assays has a pK_a of 6.8, which is at the low end of the physiological pH range. Therefore, we instead incubated 100 nM purified 0N3R tau protein, a developmental tau isoform that contains three MT-binding repeats with 0.5 µM paclitaxel-stabilized MTs in a MOPS-based buffer (pK_a = 7.2) that provides better buffering capacity in the relevant range. MT-bound tau was then separated from soluble tau protein by centrifugation through a glycerol cushion. Nearly all tau bound to MTs at pH 7.1 (99.5 ± 0.2%; mean ± SD; Fig. 2A). In contrast, the amount of tau in the MT pellet was significantly reduced at pH 7.8 to 91.7 ± 3.4%, and a detectable fraction of unbound tau remained in the supernatant.

Because this was a relatively small difference likely due to near saturation of the binding reaction at these concentrations, we next determined the apparent dissociation constant (K_d) of tau-MT binding at pH 7.1 and pH 7.8. To quantify the amount of MT-bound tau protein more accurately than we were able to achieve by immunoblot and densitometry, we instead used a fluorescently tagged 0N3R sfGFP-tau. The fraction of MT-bound sfGFP-tau was determined by measuring the fluorescence of sfGFP-tau that remained in the supernatant and that co-sedimented with MTs, varying the MT concentration over approximately two orders of magnitude around the anticipated K_d (32). Using hyperbolic curve fitting to a binding isotherm, we calculated a K_d of 0.11 ± 0.014 µM (mean ± SD; Fig. 2B) at pH 7.1. This reflects a slightly higher 0N3R affinity for MTs compared to reported values (32), which may be due to our different and lower salt buffer conditions. Importantly however, at pH 7.8, the measured K_d was significantly increased by approximately 2-fold (0.2 ± 0.013 µM) indicating that the affinity of tau for MTs is decreased at increased pH within the physiological intracellular pH range.

Intracellular pH modulates tau-MT binding in cells

In vitro experiments cannot fully reconstitute the intracellular milieu or the effect of posttranslational modifications (10). In addition, taxanes used to stabilize MTs *in vitro* alter tau-MT interactions (33). We therefore next asked whether changes in pH_i alter tau-MT binding in human retinal pigment epithelial (RPE) cells transiently expressing mEmerald-tagged 0N3R tau (Em-tau) at a low level that did not induce MT bundling. pH_i changes were measured in parallel in untransfected cells (34, 35). In control pH 7.4 HEPES buffer, the pH_i of RPE cells was ~7.4 and Em-tau clearly bound along MTs although a substantial fraction of Em-tau remained in the cytoplasm. Acute increase of pH_i to ~7.7 by addition of 20 mM NH_4Cl resulted in a notable decrease in MT-bound tau (Fig. 3A; supplementary Video S2). Because of low amounts of MT-bound tau at high pH_i and movement of the MT network in these time-lapse sequences, direct measurements of MT-bound tau were difficult and unreliable. Therefore, we instead quantified Em-tau fluorescence intensity in the cytoplasm. It is important to note that the reported pKa of mEmerald is ~6.0 and mEmerald fluorescence is virtually insensitive to pH changes above 7.0 (36). Indeed, we did not observe an increase in total cell fluorescence when pH_i was increased within the physiological range. Thus, the observed increase in cytoplasm Em-tau fluorescence in response to experimentally increased pH_i reflects dissociation from MTs. Em-tau dissociation from MTs occurred within seconds and was rapidly reversed when the NH_4Cl

solution was washed out and replaced with control HEPES buffer lowering pH_i to its normal value.

In contrast, the MT network was not affected by these acute pH_i changes as quantified by measuring the cytoplasm fluorescence intensity of EGFP-tagged tubulin not incorporated into MTs (Fig. 3). This demonstrates that Em-tau dissociation from MTs at elevated pH_i was not a consequence of MT depolymerization, and that the overall polymerization state of the MT network is insensitive to short-term pH_i changes within this range although we did not directly test MT plus end growth dynamics.

We observed a similar rapid and reversible disruption of Em-tau binding to MTs when pH_i was acutely increased with 100 mM NaCl (Fig. 4), which osmotically activates proton efflux by the plasma membrane Na^+-H^+ exchanger NHE1 (34, 35). Tau belongs to the MAP2/tau family of microtubule-associated proteins (MAPs) that share the same repeat motif in the MT-binding domain (1), and the histidine residues at the C-termini of MT-binding repeats in all these proteins are remarkably conserved (Fig. 1D). To test whether other MAP2/tau family proteins respond to intracellular pH_i changes, we transiently expressed the MT-binding region of mouse MAP4 containing three MT-binding repeats in RPE cells. Like Em-tau, Em-MAP4 responded to hyperosmotic pH_i increase with a reversible decrease in MT-binding (Fig. 4) indicating that decreased MT binding at increased pH_i may be a common characteristic of MAP2/tau family proteins.

The above experiments relied on acute changes in pH_i that occur within seconds to minutes. To test how long-term pH_i changes affected tau-MT interactions, we transiently expressed Em-tau in MCF10A mammary epithelial cells stably expressing an estrogen receptor-induced oncogenic H-RasV12 (ER-RasV12). We previously showed that tamoxifen-induced RasV12 expression increased pH_i to almost 7.7 within 24 hours (37). We found that Em-tau was predominantly cytosolic in tamoxifen-induced RasV12-expressing cells. However, acutely decreasing pH_i with a pH 7.2 buffer containing the protonophore nigericin, which equilibrates extracellular and intracellular pH, resulted in a rapid rescue of Em-tau binding to MTs (Fig. 5). Together these data demonstrate that

an increase in pH_i within the physiological range weakens tau-MT binding, which in cells results in substantially decreased MT-associated tau.

Histidines confer pH sensitivity and are required for interactions with MTs

The location of His299 within a hydrophobic pocket indicates that hydrophobic interactions of the histidine aromatic ring are important for MT binding, and may explain the high degree of conservation of these histidine residues. To further investigate this, we sought to identify mutations that mimic $His299^0$ and $His299^+$ in a pH-independent manner. We therefore built a model in which His299 was changed to a constitutively positively charged lysine residue that we hypothesized could mimic $His299^+$. However, MD simulations showed that a lysine substitution behaved more like deprotonated $His299^0$ (supplementary Fig. S1). While protonated lysine cation-π interactions are strong and commonly observed in proteins (38), due to the high entropic desolvation cost, the β tubulin hydrophobic cleft near Phe395 and Phe399 cannot readily accommodate the hydrophilic lysine ammonium cation. In fact, Lys299 turns away from the hydrophobic cleft although it can maintain electrostatic interactions with Glu422 (Fig. 6A).

To further evaluate the importance of hydrophobic contacts by *in silico* MD, we next analyzed a substitution of His299 with alanine, a small non-charged amino acid that is not expected to contribute to either hydrophobic or electrostatic interactions. Like lysine, the alanine substitution also showed increased fluctuations of the tau-MT complex near the C-terminus of tau R2 (supplementary Fig. S1), and throughout the MD simulation Ala299 pointed away from the hydrophobic cleft (Fig. 6A; supplementary Video S3).

While we cannot directly infer binding free energy changes from MD, our *in silico* models support that the positively charged $His299^+$ can uniquely form both an electrostatic interaction with Glu422 and an energetically favorable interaction with Phe399. In contrast, lysine at position 299 only maintains the electrostatic interaction while an Ala299 loses both resulting in partial dissociation of the tau peptide from the MT surface.

To directly test that conserved histidines are required for tau-MT-binding, we generated mutant

tau 0N3R protein in which all four histidine residues in the MT-binding repeats (R3 has two adjacent histidines) were substituted with either lysine (4H>K) or alanine (4H>A). If MT-binding relied only on electrostatic interactions with protonated histidines, tau(4H>K) MT-binding would be expected to be similar to wild-type tau, while tau(4H>A) should show reduced MT-binding. Instead, and consistent with our structural analysis, both variants displayed substantially reduced MT binding *in vitro* (Fig. 6B). Although tau(4H>K) seemed to bind to MTs somewhat better than tau(4H>A), *in vitro* this difference was not statistically significant.

If these conserved histidines are responsible for the pH sensitivity of tau-MT binding, because of the high pK_a of lysine, residual Tau(4H>K) binding to MTs should no longer respond to pH changes within the physiological range. Because the K_d values we measured for pH-modulated tau-MT binding were in the 100-200 nM range (Fig. 2B), we tested this at a 20-fold lower tau to MT ratio that should be well below saturation. At these low tau concentrations (10 nM), it was not possible to accurately determine the amount of tau remaining in the supernatant. Instead we compared how much tau was recovered in the MT pellet at pH 7.8 and pH 7.1, which was reduced to 52.8 ± 18.3% (mean ±SD; Fig. 6C). As a control, the amount of MTs in the pellet remained unchanged indicating that this difference reflects tau-MT-binding and not a decrease in MT stability at higher pH. In contrast to wild-type tau, MT-binding of tau(4H>K) was not decreased at increased pH (112.5 ± 8.1%; Fig. 6C), and the pH 7.8 to pH 7.1 ratio was not significantly different from the amount of MTs recovered in the pellet.

Lastly, we tested binding of fluorescently tagged tau variants to MTs in RPE cells expressing equivalent levels of wild-type or mutated Em-tau (Fig. 7; supplementary Fig. S2). In cells, binding of Em-tau(4H>K) to MTs was significantly reduced compared with wild-type tau, and Em-tau(4H>A) did not bind MTs at all. Together, these data confirm that conserved histidine residues in the tau MT-binding repeats are required for tau MT-binding that are not solely explained by electrostatics, and protonation of these histidines can be titrated to modulate tau-MT interactions.

DISCUSSION

We used multiple approaches including MD simulations and MT binding assays *in vitro* and in cells to show that interactions of MAP2/tau family proteins with MTs are sensitive to pH changes within the physiological intracellular range. We also demonstrate that histidine residues near the C-terminal end of MAP2/tau family MT-binding repeats are essential. Tau mutants with these histidines substituted with either lysine or alanine show reduced or completely absent MT-binding in cells. In addition, at least *in vitro* these conserved histidines mediate pH sensitivity as replacing them with lysine residues, which are insensitive to pH changes in the physiological range, abolishes pH-modulation of MT-binding *in vitro*. However, we were not able to test this rigorously in cells because of the already substantially reduced MT-binding of the H>K mutant.

Although these MAP2/tau MT-binding repeat histidine residues are highly conserved, their importance has not been recognized because the intrinsically disordered nature of MAP2/tau family proteins complicates structural analysis. Previous studies did not resolve MT-bound peripheral regions of these MT-binding repeats and predominantly found MAP2/tau family densities along the MT protofilament ridge (2). Although a high-definition model of native MT-bound tau is still not available, recent cryo-EM data of MT-bound constructs of human tau MT-binding repeat R2 show a close interaction of His299 with the tubulin interdimer interface (28). This overall arrangement of tau histidine residues near tubulin-tubulin interfaces is also supported by NMR and more recent electron paramagnetic resonance spectroscopy data (30, 39).

At low pH, our structural and MD analysis defines a stable interaction of the protonated histidine with specific aromatic residues in β-tubulin H11. This requires the amphiphilic character of protonated histidine as deprotonation at high pH or substitution with either non-aromatic or non-charged amino acids substantially weakens tau-MT interactions. Thus, our data are consistent with older biochemical crosslinking data showing tau interaction with H11, H12 and the flexible loop connecting these helices (40) and new ultrastructural analysis of MT-bound MAP4 that indicates a strong contribution of the tubulin

interdimer interface to the overall MAP4-MT binding energy (41).

Cation-π interactions between aromatic rings and positive charges are common in proteins, and histidine-aromatic complexes are energetically favorable in the hydrophobic protein interior (38, 42, 43). Despite its unusual arrangement for a cation-π interaction with the edge of Phe399 pointing toward the His299 ring, we find that protonated His299$^+$ maintains this proximity and geometry throughout 5 ns MD simulations. Given that the positive charge is not located above the π system, we propose that this unusual geometry may be stabilized by additional electrostatics. The Amber force field used in our simulations does not explicitly compute cation-π interactions, but it indirectly accounts for them by including both electrostatics and van-der-Waals energies. Our MD calculations are focused on how tau-MT interactions are modulated, but it is plausible that His299 protonation influences the unbound tau conformation, which could contribute to tau-MT net binding affinities. However, quantitative estimates of such relative free energies are challenging and were not attempted here.

Because of its role in neurodegenerative disease, tau is the most widely studied member of the MAP2/tau family, and much research has focused on the role of tau aggregation in Alzheimer's disease and related tauopathies with over 14000 publications listed in PubMed (3). Less is known about how MAP2/tau family proteins control the MT cytoskeleton in normal neurons. *In vitro*, tau promotes MT polymerization and protects MTs from disassembly likely by spanning multiple tubulin dimers and thus inhibiting their dissociation. Consequently, MAP2/tau family proteins are thought to stabilize MTs in neurons. Recent data of shRNA-mediated tau depletion in primary neurons indicate that tau promotes growth cone MT elongation (44). In addition, tau inhibits EB1 association with growing MT ends (45) suggesting a multiple roles of tau in controlling neuronal MT polymerization dynamics. High levels of MAP2/tau family proteins induce MT bundles in non-neuronal cells with inter-MT spacing similar to neurite MT bundles (6). Binding of MAP2/tau family proteins along MTs also inhibits MT motor movements (5). However, these functional data rely mostly on *in vitro* experiments or MAP2/tau protein overexpression, and to what extent these reflect physiological neuronal tau functions remains unclear. For example, MT-based transport appears unaffected in tau knock-out mice (46), and moderate tau expression levels have little effect on MT network organization. In summary, much remains to be learned about how MAP2/tau proteins control physiologically normal neuronal MT cytoskeleton function. What we do know though is that neurons are morphologically complex and thus the activity of neuronal cytoskeleton proteins must be controlled precisely.

Characteristic of many intrinsically disordered proteins are their complex phosphorylation patterns. MAP2/tau proteins are no exception (3, 47) and phosphorylation within the MT-binding repeats generally reduces tau MT-binding, consistent with electrostatic repulsion between negatively charged phosphates and the strong negative electrostatic field of the MT surface. We propose that the upshifted pK$_a$ of the conserved MT-binding repeat histidine residues allows them to act as pH sensors and modulate tau-MT electrostatic interactions within the physiological pH range. Consistent with a decreased tau-MT interaction strength, individual tau molecules also show increased diffusion along MTs at increased pH (48). Thus, pH$_i$ changes may add another layer of control to MAP2/tau MT-binding. Observed differences in the magnitude of pH-modulated tau MT-binding between our experiments *in vitro* and in cells may be due to partial phosphorylation of tau in cells. However, tau-binding to MTs is also sensitive to subtle changes in MT lattice geometry (33). Although we find that the total MT polymer is insensitive to short-term pH$_i$ changes, we cannot rule out that pH-mediated conformational changes of the MT wall contribute to pH-sensitive tau-MT interactions.

Currently, we can only speculate as to the physiological relevance of pH modulating tau-MT-binding. Because neurons are morphologically differentiated with highly compartmentalized cytoplasm, it is possible that developmental or spatial control of pH$_i$ in developing neurons contributes to spatiotemporal control of MAP2/tau activities, but potential local differences in neuronal cytoplasmic pH$_i$ remain poorly characterized (49, 50). However, acidification of the neuronal cytoplasm has been associated with and speculated to be a causative

agent in neurodegeneration (21). Our current data would predict enhanced tau-MT binding in acidified neurons, which is inconsistent with tau aggregation due to weakened tau-MT interactions in Alzheimer's disease. Alternatively, increased binding of protonated tau to negatively charged phospholipid membranes may increase toxic effects of aggregated tau (51).

Lastly, ectopic tau expression has been described in many types of cancer and elevated tau levels appear to correlate with aggressive metastatic cancer phenotypes and resistance to taxane chemotherapy (52–54). Cancer cells generally have elevated pH_i (19, 20) although a large variability in different types of cancers is likely. Our data indicate that tau-MT-binding is greatly reduced in a breast cancer model driven by oncogenic RasV12 and is rapidly rescued by returning pH_i to a physiological normal level. Thus, we would predict that taxane sensitivity positively correlates with pH_i in tau-expressing cancers, which could serve as a diagnostic tool for taxane chemotherapy. In conclusion, even though we do not yet understand the functional relevance of pH-modulated tau-MT interactions in normal or pathological conditions, the current study adds another facet to the already complex regulation of MAP2/tau cell biology.

EXPERIMENTAL PROCEDURES

Molecular dynamics – The recently reported cryo-EM structure of MT-bound tau MT-binding repeat 2 (amino acids 274-300; PDB ID: 6CVN) was used as starting point for MD simulations (28). The pK_a of MT-bound His299 was predicted using the PROPKA3 software (29). Two different protonation states for His299 were modeled, a neutral $His299^0$ protonated on the ε nitrogen, as predicted by the Maestro Protein Preparation package, and a double protonated form, $His299^+$. His299 was also mutated to lysine or alanine using the 'swappa' command as implemented in Chimera (55). Preceding MD simulations, the tau-MT model structures were submitted to 1,000 steps of steepest descent minimization, followed by 1,000 ps of equilibration. The SHAKE algorithm was used to constrain all bonds containing hydrogen atoms. A cut-off of 12 Å was used for long-range interactions. These energy-minimized models were then submitted to short time MD simulations (5 ns) using the NPT ensemble with the Amberff12SB force field (56). The Berendsen pressure coupling scheme was used for keeping the pressure constant at 1 atm. The temperature of the production was constant at 310K using the Langevin thermostat.

Plasmids and protein production – Mammalian expression plasmids mEmerald-MAPTau-C-10 (encoding full-length human tau isoform 4; accession number NM_016841) and mEmerald-MAP4-C-10 (containing the MAP4 the -binding domain; Addgene Plasmid # 54152) were from the Michael Davidson plasmid collection. Tau(4H>K) and (4H>A) mutations were constructed as gene blocks (Integrated DNA Technologies) and inserted into the wildtype pmEmerald-MAPTau-C-10 plasmid using Gibson assembly. For bacterial expression, full length 0N3R tau was subcloned into a pET28a bacterial expression vector using Gibson assembly containing an N-terminal 6xHis-tag. sfGFP-tau was constructed with an N-terminal 6xHis-tag and tandem Strep-tags connected by a GS-linker, followed by sfGFP, a precision protease cleavage site, and the 0N3R tau sequence.

Tau proteins were expressed in BL21(DE3) *E. coli* cells in Luria Broth after induction with 0.4-1 mM isopropyl β-D-1-thiogalactopyranoside (IPTG) overnight at 18°C. For 6xHis-tau, bacteria pellets were lysed by sonication on ice in 50 mM Tris-HCl pH 7.5, 150 mM NaCl, 1 mM DTT and protease inhibitors. 6xHis-tau was purified by affinity chromatography on Ni-NTA resin, eluted into 50 mM Tris-HCl pH 7.8, 200 mM NaCl, 200 mM imidazole, then dialyzed into 20 mM Tris-HCl pH 7.4, 150 mM NaCl, 10% glycerol, 1 mM DTT. For sfGFP-tau, bacteria pellets were resuspended in 50 mM Tris-HCl pH 8.0, 2 mM $MgCl_2$, 1mM EGTA, and 10% glycerol and lysed using an Emulsiflex C3 (Avestin). sfGFP-tau was purified by affinity chromatography on Strep XT beads (IBA Lifesciences), followed by anion exchange chromatography on a HiTrap Q HP column in 50 mM Tris-HCl pH 7.5, 2 mM $MgCl_2$, 1mM EGTA, and 10% glycerol with a linear salt gradient from 100 mM to 400 mM, and finally by size exclusion chromatography on a Superose 6 in 50 mM Tris-HCl pH 8.0, 2 mM $MgCl_2$, 1mM EGTA, and 10% glycerol. Tau proteins were concentrated to ~50 μM, and aliquots were flash frozen in liquid N_2 and stored at -80°C.

In vitro MT-binding assays – Paclitaxel-stabilized MTs were prepared by polymerizing 25 μM purified porcine or bovine tubulin in 80 mM K-PIPES pH 6.8, 5 mM $MgCl_2$, 1 mM EGTA, 33% glycerol and 1 mM GTP at 37 °C. After 30 min MTs were stabilized by addition of 50 μM paclitaxel.

To test MT-binding of histidine mutants, 100 nM tau protein was incubated with 1 μM MTs in 250 μl BRB80 (80 mM K-PIPES pH 6.8, 1 mM $MgCl_2$, 1 mM EGTA) with 1 mM DTT, 10 μM paclitaxel, and 10 μg/ml BSA. For testing pH-sensitive MT-binding *in vitro*, we instead used a MOPS-based buffer with improved buffering capacity in the physiological pH range (20 mM MOPS, 0.1 mM EDTA, 0.1 mM EGTA, 5 mM magnesium acetate, 50 mM potassium acetate) with 1mM DTT, 10 μM paclitaxel, and 10 μg/ml BSA. The MOPS buffer pH was adjusted to 7.2 and 8.0, respectively. pH values reported on the figures were measured after adding buffer equivalent to the amounts of MTs and tau added, which lowered the pH in the binding reactions by 0.1-0.2 pH units. For reactions with 10 nM tau, the volume was doubled to 500 μl. After 20 min incubation at room temperature, MT-binding reactions were overlaid onto 400-600 μl of BRB80 or the MOPS-based buffer with 10 μM paclitaxel containing 60% w/v glycerol and centrifuged in a Beckman TLA 100.2 rotor at 50,000 rpm for 20

min at 25°C. After centrifugation a portion of the supernatant (S) was saved for analysis, the cushion carefully washed with ddH$_2$O to minimize contamination of the pellet and removed, and the pellet (P) resuspended in SDS-PAGE sample buffer. Equivalent amounts of supernatant and pellet were analyzed by SDS-PAGE on 4-12% NuPage gels (Invitrogen) and immunoblotting with a tau antibody (E-4, sc-515539; Santa Cruz Biotechnology). Coomassie-stained gels and chemiluminescent immunoblots were imaged with a FluorChem Q gel documentation system (92-14116-00, Alpha Innotech). The MT-bound tau fraction was calculated as $(I_P-I_{bkg})/(I_S+I_P-I_{bkg})$.

To determine dissociation constants using sfGFP-tau fluorescence, MTs were diluted in a 1:2 dilution series into 10 µl BRB80 with 10 µM paclitaxel and mixed with 50 nM sfGFP-tau in 200 µl MOPS buffer with DTT, paclitaxel and BSA as above in 500 µl Eppendorf tubes with the lids cut off. After 20 min incubation at room temperature, the tubes with the binding reactions were set into TLA 100.2 polycarbonate tubes and centrifuged as above, but without a glycerol cushion. 150 µl supernatant was then directly transferred from the centrifuge tube into a 100 µl Sub-MicroQuartz Fluorometer Cell (Starna Cells, Inc.) to minimize sfGFP-tau loss through unspecific adhesion to plastic. After removing the remainder of the supernatant, MT pellets were resuspended in 200 µl ice-cold MOPS buffer without paclitaxel. sfGFP-tau fluorescence (F) was measured with a SpectraMax M5 plate reader (Molecular Dynamics, Sunnyvale, CA) at λ_{Ex} = 480 nm and λ_{Em} = 520 nm. The fraction of MT-bound sfGFP-tau (f_{bnd}) for each MT concentration was calculated as the average of $(F_{tot}-F_S)/F_{tot}$ in which F_{tot} is the fluorescence in the supernatant with no MTs, and $F_P/(F_S+F_P)$. Curve fitting with a binding isotherm $f_{bnd} = b_{max}\cdot[MT]/(K_d+[MT])$ was done in MATLAB (MathWorks).

Cell culture, live cell imaging and analysis – Retinal pigment epithelial (RPE) cells were maintained in RPMI medium (Invitrogen) supplemented with 10% fetal bovine serum (Atlanta Biosciences) and 1% Glutamax (Invitrogen) at 37°C, 5% CO$_2$. MCF10A cells stably expressing ER-RASV12 were maintained as described (37). For transient protein expression and microscopy, cells were plated in 35 mm glass-bottom dishes (MatTek), transfected after 24 h using Fugene6 (Promega) and 1 µg plasmid DNA, and used for experiments 24 h later after replacing the transfection medium.

To determine the pH response of tau MT-binding in cells, the tissue culture medium was replaced with 25 mM Na-HEPES pH 7.4, 140 mM NaCl, 5 mM KCl, 10 mM glucose, 1 mM MgSO$_4$, 1 mM K$_2$HPO$_4$/KH$_2$PO$_4$ (pH 7.4), and 2 mM CaCl$_2$. Cells were imaged on an environmentally controlled spinning disk confocal system as described (57, 58). After 3-5 images in the control HEPES pH 7.4 buffer, the buffer was replaced with the same buffer either containing 20 mM NH$_4$Cl or 100 mM NaCl. After 5-10 min the buffer was once again replaced with control HEPES buffer. Intracellular pH changes with these treatments were determined in parallel in untransfected cells loaded with 2,7-biscarboxyethyl-5(6)-carboxyfluorescein (BCECF) essentially as described (34, 35). BCECF fluorescence at λ_{Em} = 530 nm at two different excitation wavelengths (λ_{Ex} = 440 nm and 490 nm) were acquired using the SpectraMax M5 plate reader and calibrated to cells treated with 10 µM of the proton ionophore nigericin (Invitrogen) at pH 7.5 and pH 6.6.

To indirectly analyze the amount of MT-bound tau at different pH$_i$ values, we measured the mEmerald-tau fluorescence in the cytoplasm, which increases if less tau is MT-bound. mEmerald fluorescence intensity was measured in three small regions-of-interest (ROIs) per cell in three different time-points on the unprocessed 16-bit images per buffer condition, and as necessary, the ROIs were moved slightly between images to avoid MT movements. ROI intensities were corrected for photobleaching or potential pH-dependent changes in mEmerald fluorescence by normalizing to the total cell fluorescence in the first captured image. Normalization to the first time point also preserved variability between measurements. The relative amount of MT-bound tau mutants was quantified as described (33). All image analysis was done in NIS Elements version 4.3 or higher (Nikon). Significance of multiple comparisons was calculated by Tukey–Kramer honest significant difference (HSD) test in Analyse-It for Microsoft Excel. Figures were assembled in Adobe Illustrator CS5, and videos were made using Apple QuickTime Pro. Box-and-whisker plots show median, first and third quartile,

observations within 1.5 times the interquartile range, and all individual data points.

Acknowledgements:

Conflict of interest:

The authors declare that they have no conflicts of interest with the contents of this article.

Author contributions:

R.C., D.L.B. and T.W designed experiments and analyzed data. R.C. performed in vitro biochemistry. D.L.B. performed experiments in cells. P.L. contributed to experiments. W.A.C. and M.P.J. performed molecular dynamics simulations and structural analysis. R.T. and R.J.M. prepared sfGFP-tau protein. R.C., D.L.B., W.A.C, M.P.J., and T.W. contributed to writing of the manuscript.

REFERENCES

1. Dehmelt, L., and Halpain, S. (2004) The MAP2/Tau family of microtubule-associated proteins. *Genome Biol.* **6**, 204

2. Al-Bassam, J., Ozer, R. S., Safer, D., Halpain, S., and Milligan, R. A. (2002) MAP2 and tau bind longitudinally along the outer ridges of microtubule protofilaments. *J. Cell Biol.* **157**, 1187–1196

3. Wang, Y., and Mandelkow, E. (2016) Tau in physiology and pathology. *Nat. Rev. Neurosci.* **17**, 5–21

4. Qiang, L., Yu, W., Andreadis, A., Luo, M., and Baas, P. W. (2006) Tau Protects Microtubules in the Axon from Severing by Katanin. *J. Neurosci.* **26**, 3120–3129

5. Dixit, R., Ross, J. L., Goldman, Y. E., and Holzbaur, E. L. F. (2008) Differential regulation of dynein and kinesin motor proteins by tau. *Science*. **319**, 1086–1089

6. Chen, J., Kanai, Y., Cowan, N. J., and Hirokawa, N. (1992) Projection domains of MAP2 and tau determine spacings between microtubules in dendrites and axons. *Nature*. **360**, 674–677

7. Kovacs, G. G. (2015) Invited review: Neuropathology of tauopathies: principles and practice. *Neuropathol. Appl. Neurobiol.* **41**, 3–23

8. Goedert, M. (2018) Tau filaments in neurodegenerative diseases. *FEBS Lett.* **592**, 2383–2391

9. Ramkumar, A., Jong, B. Y., and Ori-McKenney, K. M. (2018) ReMAPping the microtubule landscape: How phosphorylation dictates the activities of microtubule-associated proteins. *Dev. Dyn.* **247**, 138–155

10. Ross, J. L. (2016) The Dark Matter of Biology. *Biophys. J.* **111**, 909–916

11. Schönichen, A., Webb, B. A., Jacobson, M. P., and Barber, D. L. (2013) Considering Protonation as a Posttranslational Modification Regulating Protein Structure and Function. *Annu. Rev. Biophys.* **42**, 289–314

12. Putney, L. K., and Barber, D. L. (2003) Na-H Exchange-dependent Increase in Intracellular pH Times G2/M Entry and Transition. *J. Biol. Chem.* **278**, 44645–44649

13. Flinck, M., Kramer, S. H., Schnipper, J., Andersen, A. P., and Pedersen, S. F. (2018) The acid-base transport proteins NHE1 and NBCn1 regulate cell cycle progression in human breast cancer cells. *Cell Cycle*. **17**, 1056–1067

14. Choi, C.-H., Webb, B. A., Chimenti, M. S., Jacobson, M. P., and Barber, D. L. (2013) pH sensing by FAK-His58 regulates focal adhesion remodeling. *J. Cell Biol.* **202**, 849–859

15. Ludwig, F. T., Schwab, A., and Stock, C. (2013) The Na+/H+-exchanger (NHE1) generates pH nanodomains at focal adhesions. *J. Cell. Physiol.* **228**, 1351–1358

16. Denker, S. P., and Barber, D. L. (2002) Cell migration requires both ion translocation and cytoskeletal anchoring by the Na-H exchanger NHE1. *J. Cell Biol.* **159**, 1087–1096

17. Hayashi, H., Aharonovitz, O., Alexander, R. T., Touret, N., Furuya, W., Orlowski, J., and Grinstein, S. (2008) Na+ /H+ exchange and pH regulation in the control of neutrophil chemokinesis and chemotaxis. *Am. J. Physiol. Physiol.* **294**, C526–C534

18. Lauritzen, G., Stock, C. M., Lemaire, J., Lund, S. F., Jensen, M. F., Damsgaard, B., Petersen, K. S., Wiwel, M., Rønnov-Jessen, L., Schwab, A., and Pedersen, S. F. (2012) The Na+/H+exchanger NHE1, but not the Na+, HCO3- cotransporter NBCn1, regulates motility of MCF7 breast cancer cells expressing constitutively active ErbB2. *Cancer Lett.* **317**, 172–183

19. Webb, B. A., Chimenti, M., Jacobson, M. P., and Barber, D. L. (2011) Dysregulated pH: A perfect storm for cancer progression. *Nat. Rev. Cancer*. **11**, 671–677

20. White, K. A., Grillo-Hill, B. K., and Barber, D. L. (2017) Cancer cell behaviors mediated by dysregulated pH dynamics at a glance. *J. Cell Sci.* **130**, 663–669

21. Majdi, A., Mahmoudi, J., Sadigh-Eteghad, S., Golzari, S. E. J., Sabermarouf, B., and Reyhani-Rad, S. (2016) Permissive role of cytosolic pH acidification in neurodegeneration: A closer look at its causes and consequences. *J. Neurosci. Res.* **94**, 879–887

22. Harguindey, S., Stanciu, D., Devesa, J., Alfarouk, K., Cardone, R. A., Polo Orozco, J. D., Devesa, P., Rauch, C., Orive, G., Anitua, E., Roger, S., and Reshkin, S. J. (2017) Cellular acidification as a

new approach to cancer treatment and to the understanding and therapeutics of neurodegenerative diseases. *Semin. Cancer Biol.* **43**, 157–179

23. Srivastava, J., Barreiro, G., Groscurth, S., Gingras, A. R., Goult, B. T., Critchley, D. R., Kelly, M. J. S., Jacobson, M. P., and Barber, D. L. (2008) Structural model and functional significance of pH-dependent talin-actin binding for focal adhesion remodeling. *Proc. Natl. Acad. Sci. U S A*. **105**, 14436–14441

24. White, K. A., Hill, B. K. G., Esquivel, M., Peralta, J., Bui, V. N., Chire, I., and Barber, D. L. (2018) β-Catenin is a pH sensor with decreased stability at higher intracellular pH. *J. Cell Biol.* **217**, 1–12

25. White, K. A., Ruiz, D. G., Szpiech, Z. A., Strauli, N. B., Hernandez, R. D., Jacobson, M. P., and Barber, D. L. (2017) Cancer-associated arginine-to-histidine mutations confer a gain in pH sensing to mutant proteins. *Sci. Signal.* **10**, eaam9931

26. Lee, S. A., Eyeson, R., Cheever, M. L., Geng, J., Verkhusha, V. V., Burd, C., Overduin, M., and Kutateladze, T. G. (2005) Targeting of the FYVE domain to endosomal membranes is regulated by a histidine switch. *Proc. Natl. Acad. Sci. U S A*. **102**, 13052–13057

27. Frantz, C., Karydis, A., Nalbant, P., Hahn, K. M., and Barber, D. L. (2007) Positive feedback between Cdc42 activity and H+ efflux by the Na-H exchanger NHE1 for polarity of migrating cells. *J. Cell Biol.* **179**, 403–410

28. Kellogg, E. H., Hejab, N. M. A., Poepsel, S., Downing, K. H., DiMaio, F., and Nogales, E. (2018) Near-atomic model of microtubule-tau interactions. *Science*. **360**, 1242–1246

29. Olsson, M. H. M., SØndergaard, C. R., Rostkowski, M., and Jensen, J. H. (2011) PROPKA3: Consistent treatment of internal and surface residues in empirical pKa predictions. *J. Chem. Theory Comput.* **7**, 525–537

30. Kadavath, H., Hofele, R. V., Biernat, J., Kumar, S., Tepper, K., Urlaub, H., Mandelkow, E., and Zweckstetter, M. (2015) Tau stabilizes microtubules by binding at the interface between tubulin heterodimers. *Proc. Natl. Acad. Sci. U S A*. **112**, 7501–7506

31. Butner, K. A., and Kirschner, M. W. (1991) Tau protein binds to microtubules through a flexible array of distributed weak sites. *J. Cell Biol.* **115**, 717–730

32. Roger, B., Al-Bassam, J., Dehmelt, L., Milligan, R. A., and Halpain, S. (2004) MAP2c, but not tau, binds and bundles F-actin via its microtubule binding domain. *Curr. Biol.* **14**, 363–371

33. Ettinger, A., van Haren, J., Ribeiro, S. A., and Wittmann, T. (2016) Doublecortin Is Excluded from Growing Microtubule Ends and Recognizes the GDP-Microtubule Lattice. *Curr. Biol.* **26**, 1549–1555

34. Meima, M. E., Webb, B. A., Witkowska, H. E., and Barber, D. L. (2009) The sodium-hydrogen exchanger NHE1 is an Akt substrate necessary for actin filament reorganization by growth factors. *J. Biol. Chem.* **284**, 26666–26675

35. Webb, B. A., White, K. A., Grillo-Hill, B. K., Schönichen, A., Choi, C., and Barber, D. L. (2016) A histidine cluster in the cytoplasmic domain of the Na-H exchanger NHE1 confers pH-sensitive phospholipid binding and regulates transporter activity. *J. Biol. Chem.* **291**, 24096–24104

36. Shaner, N. C., Steinbach, P. A., and Tsien, R. Y. (2005) A guide to choosing fluorescent proteins. *Nat. Methods*. **2**, 905–909

37. Grillo-Hill, B. K., Choi, C., Jimenez-Vidal, M., and Barber, D. L. (2015) Increased H+ efflux is sufficient to induce dysplasia and necessary for viability with oncogene expression. *Elife*. **2015**, 1–31

38. Kumar, K., Woo, S. M., Siu, T., Cortopassi, W. A., Duarte, F., and Paton, R. S. (2018) Cation-π interactions in protein-ligand binding: Theory and data-mining reveal different roles for lysine and arginine. *Chem. Sci.* **9**, 2655–2665

39. Martinho, M., Allegro, D., Huvent, I., Chabaud, C., Etienne, E., Kovacic, H., Guigliarelli, B., Peyrot, V., Landrieu, I., Belle, V., and Barbier, P. (2018) Two Tau binding sites on tubulin revealed by thiol-disulfide exchanges. *Sci. Rep.* **8**, 13846

40. Chau, M. F., Radeke, M. J., de Inés, C., Barasoain, I., Kohlstaedt, L. A., and Feinstein, S. C.

(1998) The microtubule-associated protein tau cross-links to two distinct sites on each α and β tubulin monomer via separate domains. *Biochemistry*. **37**, 17692–17703

41. Shigematsu, H., Imasaki, T., Doki, C., Sumi, T., Aoki, M., Uchikubo-Kamo, T., Sakamoto, A., Tokuraku, K., Shirouzu, M., and Nitta, R. (2018) Structural insight into microtubule stabilization and kinesin inhibition by Tau family MAPs. *J. Cell Biol.* 10.1083/jcb.201711182

42. Gallivan, J. P., and Dougherty, D. A. (1999) Cation-pi interactions in structural biology. *Proc. Natl. Acad. Sci. U S A*. **96**, 9459–9464

43. Liao, S. M., Du, Q. S., Meng, J. Z., Pang, Z. W., and Huang, R. B. (2013) The multiple roles of histidine in protein interactions. *Chem. Cent. J.* **7**, 44

44. Biswas, S., and Kalil, K. (2018) The microtubule associated protein tau mediates the organization of microtubules and their dynamic exploration of actin-rich lamellipodia and filopodia of cortical growth cones. *J. Neurosci.* **38**, 291–307

45. Ramirez-Rios, S., Denarier, E., Prezel, E., Vinit, A., Stoppin-Mellet, V., Devred, F., Barbier, P., Peyrot, V., Sayas, C. L., Avila, J., Peris, L., Andrieux, A., Serre, L., Fourest-Lieuvin, A., and Arnal, I. (2016) Tau antagonizes end-binding protein tracking at microtubule ends through a phosphorylation-dependent mechanism. *Mol. Biol. Cell*. **27**, 2924–2934

46. Yuan, A., Kumar, A., Peterhoff, C., Duff, K., and Nixon, R. A. (2008) Axonal Transport Rates In Vivo Are Unaffected by Tau Deletion or Overexpression in Mice. *J. Neurosci.* **28**, 1682–1687

47. Kimura, T., Sharma, G., Ishiguro, K., and Hisanaga, S. I. (2018) Phospho-tau bar code: Analysis of phosphoisotypes of tau and its application to tauopathy. *Front. Neurosci.* 10.3389/fnins.2018.00044

48. Hinrichs, M. H., Jalal, A., Brenner, B., Mandelkow, E., Kumar, S., and Scholz, T. (2012) Tau protein diffuses along the microtubule lattice. *J. Biol. Chem.* **287**, 38559–38568

49. Schwiening, C. J., and Willoughby, D. (2002) Depolarization-induced pH microdomains and their relationship to calcium transients in isolated snail neurones. *J. Physiol.* **538**, 371–382

50. Matlashov, M. E., Bogdanova, Y. A., Ermakova, G. V., Mishina, N. M., Ermakova, Y. G., Nikitin, E. S., Balaban, P. M., Okabe, S., Lukyanov, S., Enikolopov, G., Zaraisky, A. G., and Belousov, V. V. (2015) Fluorescent ratiometric pH indicator SypHer2: Applications in neuroscience and regenerative biology. *Biochim. Biophys. Acta - Gen. Subj.* **1850**, 2318–2328

51. Ait-Bouziad, N., Lv, G., Mahul-Mellier, A.-L., Xiao, S., Zorludemir, G., Eliezer, D., Walz, T., and Lashuel, H. A. (2017) Discovery and characterization of stable and toxic Tau/phospholipid oligomeric complexes. *Nat. Commun.* **8**, 1678

52. McGrogan, B. T., Gilmartin, B., Carney, D. N., and McCann, A. (2008) Taxanes, microtubules and chemoresistant breast cancer. *Biochim. Biophys. Acta - Rev. Cancer*. **1785**, 96–132

53. Smoter, M., Bodnar, L., Duchnowska, R., Stec, R., Grala, B., and Szczylik, C. (2011) The role of Tau protein in resistance to paclitaxel. *Cancer Chemother. Pharmacol.* **68**, 553–557

54. He, W., Zhang, D., Jiang, J., Liu, P., and Wu, C. (2014) The relationships between the chemosensitivity of human gastric cancer to paclitaxel and the expressions of class III β-tubulin, MAPT, and survivin. *Med. Oncol.* **31**, 950

55. Pettersen, E. F., Goddard, T. D., Huang, C. C., Couch, G. S., Greenblatt, D. M., Meng, E. C., and Ferrin, T. E. (2004) UCSF Chimera - A visualization system for exploratory research and analysis. *J. Comput. Chem.* **25**, 1605–1612

56. Steinbrecher, T., Latzer, J., and Case, D. A. (2012) Revised AMBER Parameters for Bioorganic Phosphates. *J. Chem. Theory Comput.* **8**, 4405–4412

57. Stehbens, S., Pemble, H., Murrow, L., and Wittmann, T. (2012) Imaging intracellular protein dynamics by spinning disk confocal microscopy. *Methods Enzymol.* **504**, 293–313

58. Ettinger, A., and Wittmann, T. (2014) Fluorescence live cell imaging. *Methods Cell Biol.* **123**, 77–94

FOOTNOTES:

The abbreviations used are: MT, microtubule; MAP, microtubule-associated protein; pH_i, intracellular pH; MD, molecular dynamics
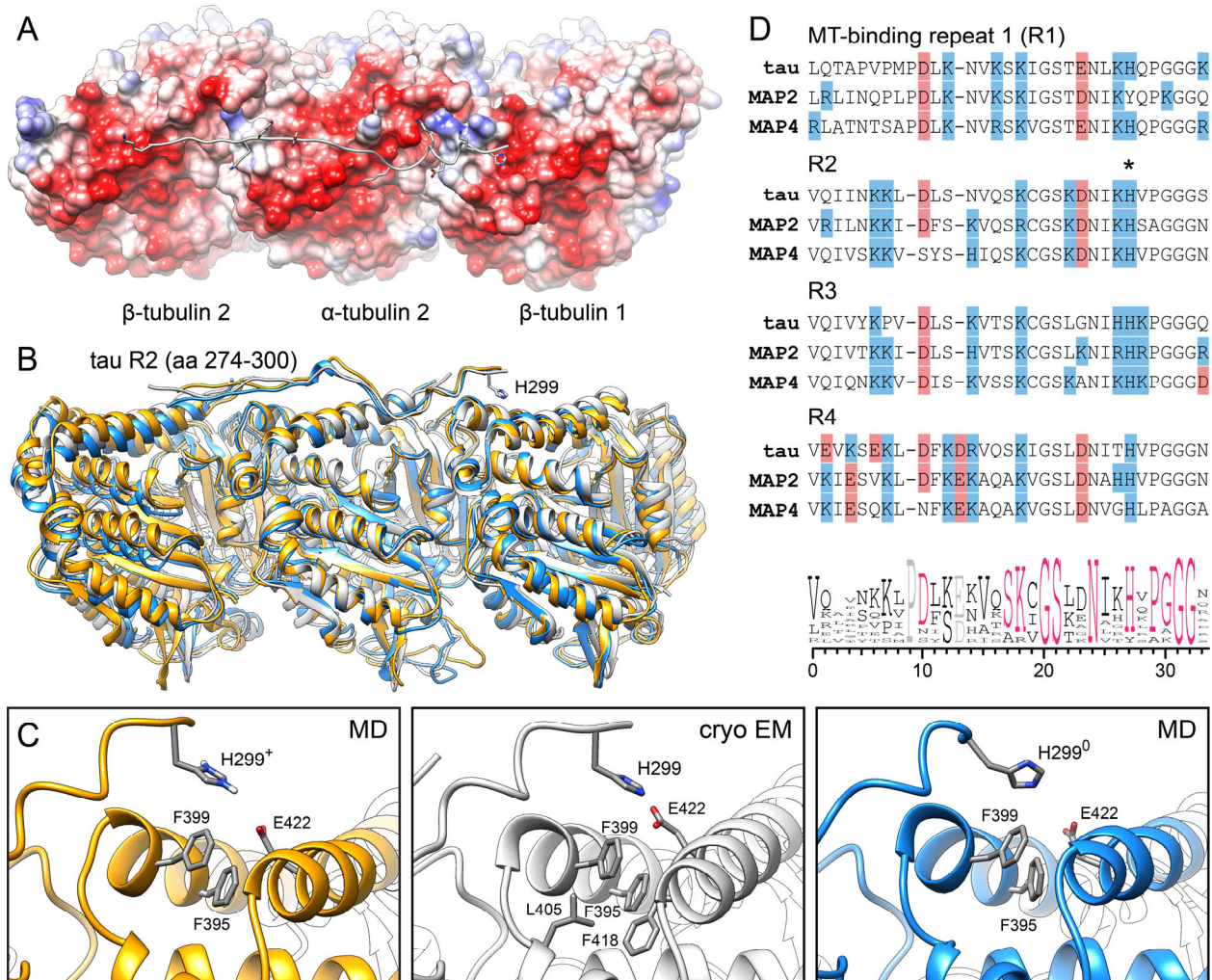
Figure 1. Molecular dynamics simulation of protonation effects on tau His299 interaction with the MT surface. (A) View of the MT-bound tau R2 MT-binding repeat from the MT outside based on the recent cryo-EM structure (PDB ID: 6CVN). The tubulin surface is colored by electrostatic potential highlighting the strongly negative surface charge or the protofilament ridge. (B) Last frames of 5 ns MD simulations of protonated $His299^+$ (i.e. low pH; orange) and unprotonated $His299^0$ (high pH; blue) compared with the cryo-EM structure (grey). A side view of the tubulin protofilament is shown with tau R2 on top. (C) Close-up views of the binding pocket surrounding His299. (D) Sequence alignment of MT-binding repeats in all members of the human MAP2/tau family indicating the high degree of conservation of the histidine residue in the position equivalent to His299 in tau R2 (asterisk).
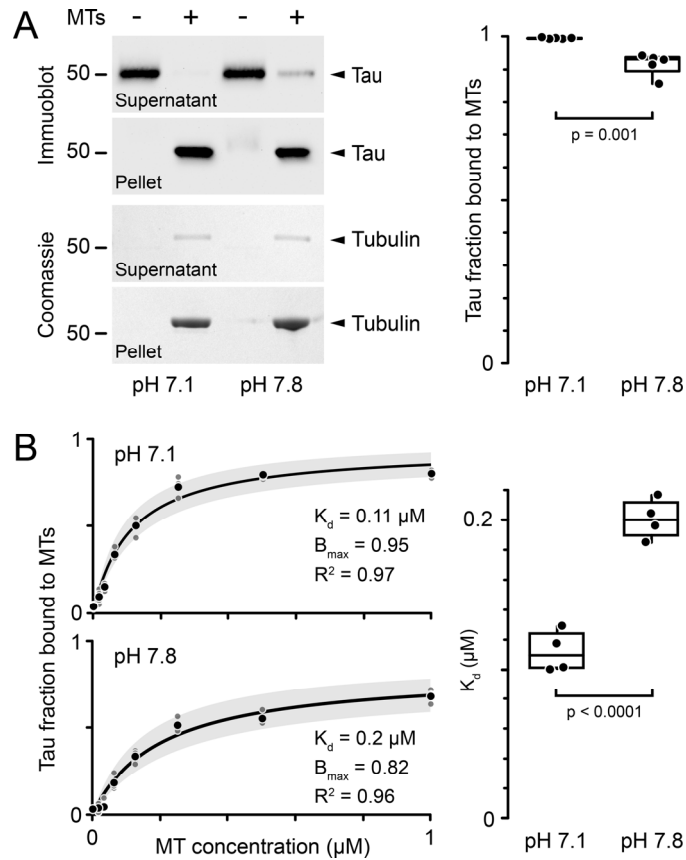
Figure 2. Increased pH decreases tau binding to MTs *in vitro*. (A) Co-sedimentation assay of 100 nM 0N3R tau protein with 0.5 µM paclitaxel-stabilized MTs. Shown are immunoblots for tau and Coomassie-stained gels for tubulin in the supernatant and pellet at the indicated pH values. Note that tau remains in the supernatant in the absence of MTs at both pH values. The boxplot shows a quantification of the tau fraction recovered in the pellet (*n* = 5). (B) Equilibrium binding of 50 nM fluorescently tagged 0N3R sfGFP-tau protein at a range of MT concentrations between 15.6 nM and 1 µM at the indicated pH values. The fraction bound was determined by MT co-sedimentation of fluorescently tagged 0N3R sfGFP-tau and measuring sfGFP-tau fluorescence in the supernatant and pellet. Grey symbols show each data point and black symbols are the average for each MT concentration. The black line shows a hyperbolic fit through data from all experiments and the grey area indicates the 95% confidence interval of the fit. The boxplot shows dissociation constants obtained when each experiment was fitted independently (*n* = 4). Box plots show median, first and third quartile, with whiskers extending to observations within 1.5 times the interquartile range, and all individual data points. Statistical analysis by Student t-test.
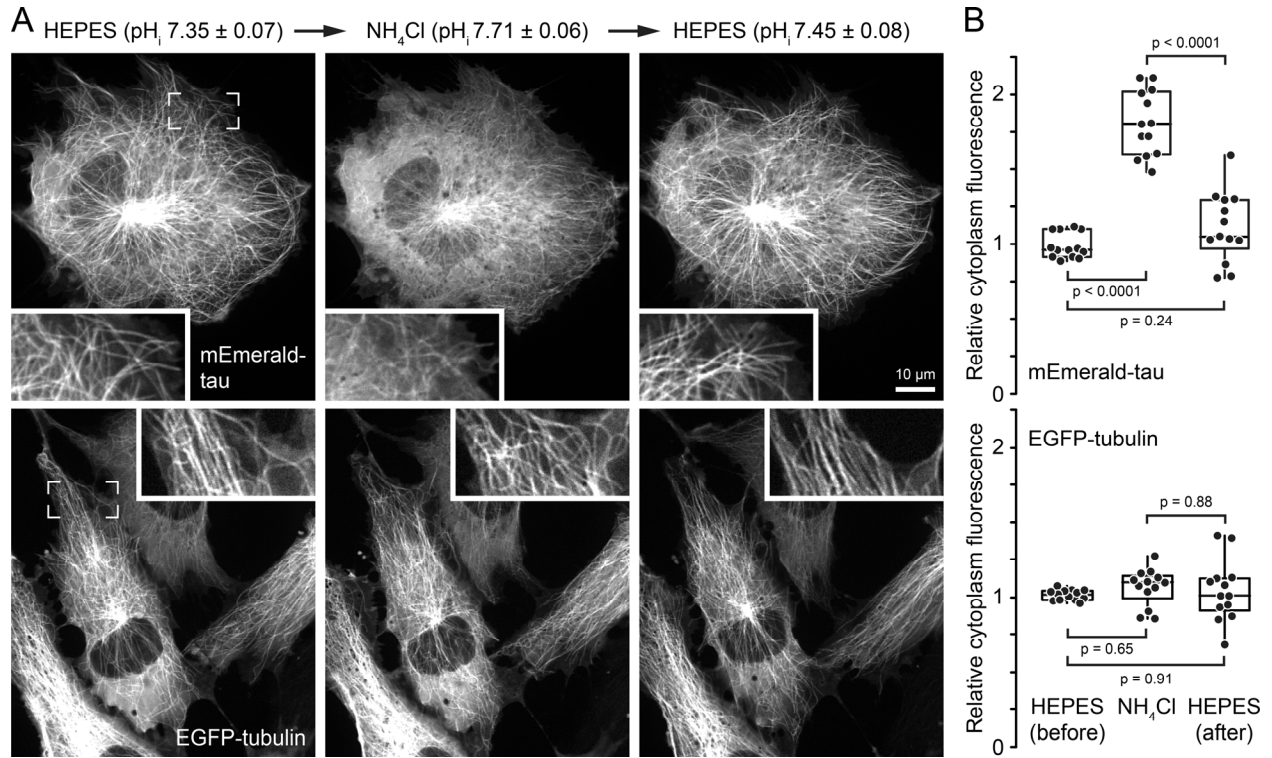
Figure 3. Increased intracellular pH decreases tau binding to MTs. (A) RPE cells transiently expressing either fluorescently tagged 0N3R tau (top row) or tubulin (bottom row) treated with 20 mM NH_4Cl to acutely increase pH_i in the cytoplasm. Insets show highlighted regions at higher magnification. (B) Quantification of the mEmerald-tau or EGFP-tubulin fluorescence in the cytoplasm (n = 13 cells each). Note that elevated pH increases mEmerald-tau signal in the cytoplasm almost 2-fold, which indicates dissociation from MTs. Box plots show median, first and third quartile, with whiskers extending to observations within 1.5 times the interquartile range, and all individual data points. Statistical analysis by Tukey-Kramer HSD test.
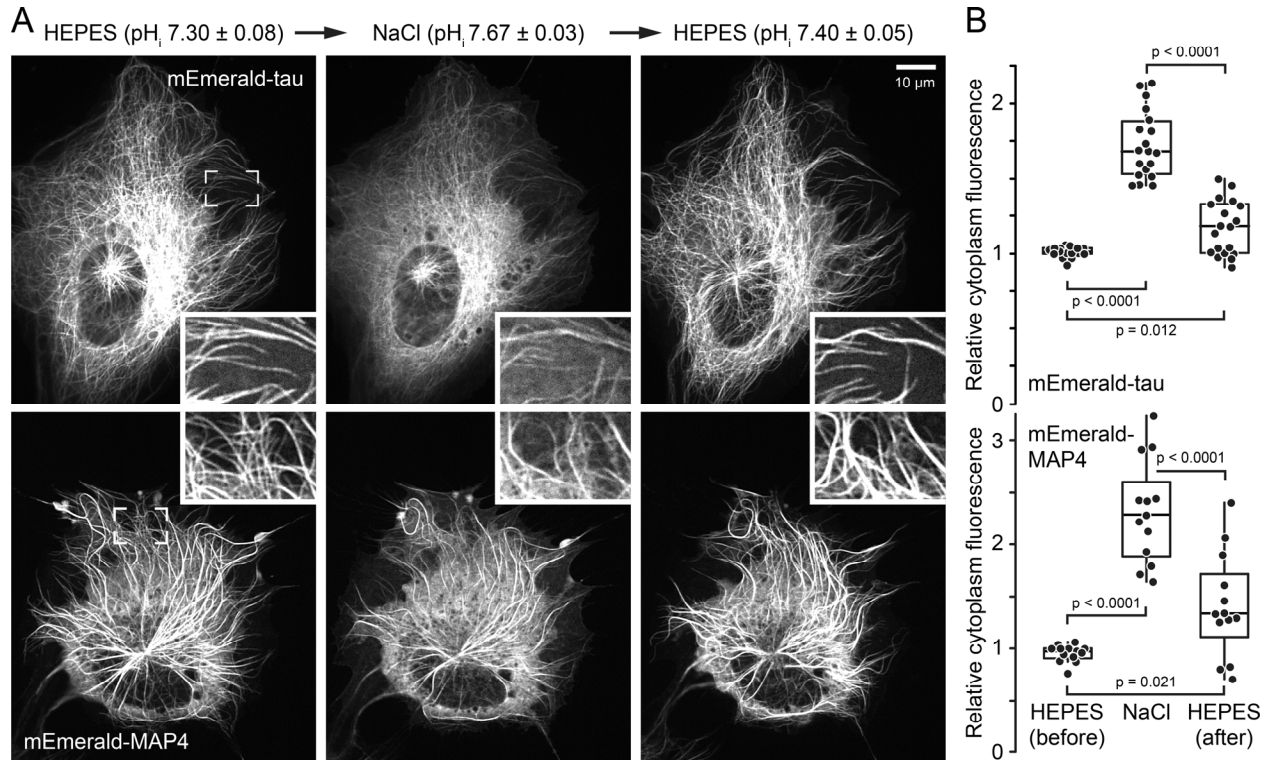
Figure 4. Increased intracellular pH decreases binding of MAP2/tau family proteins to MTs. (A) RPE cells transiently expressing either mEmerald-tagged tau (top row) or -MAP4 (bottom row) treated with 100 mM NaCl to acutely increase pH_i in the cytoplasm. Insets show highlighted regions at higher magnification. (B) Quantification of the mEmerald-tau or -MAP4 fluorescence in the cytoplasm (tau: $n = 19$; MAP4: $n = 13$ cells). Both MAP2/tau family proteins reversibly dissociate from MTs at increased pH_i. Note that MAP4 expression generally results in some degree of MT bundling, and MAP4 does not completely disappear from these bundles, but mEmerald-MAP4 in the cytoplasm is notably increased at increased pH_i. Box plots show median, first and third quartile, with whiskers extending to observations within 1.5 times the interquartile range, and all individual data points. Statistical analysis by Tukey-Kramer HSD test.
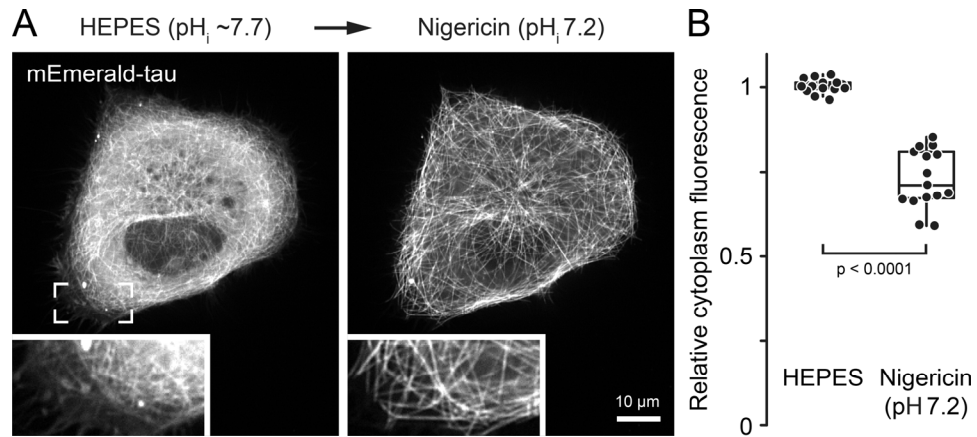
Figure 5. Decreasing pH$_i$ in cancer cells enhances tau binding to MTs. (A) MCF10A mammary epithelial cells expressing oncogenic H-RasV12 before and after treatment with a nigericin buffer to equilibrate pH$_i$ to 7.2. Inset shows highlighted regions at higher magnification. (B) Quantification of the relative mEmerald-tau fluorescence in the cytoplasm (n = 15 cells). Box plot shows median, first and third quartile, whiskers extending to observations within 1.5 times the interquartile range, and all individual data points. Statistical analysis by Student t-test.
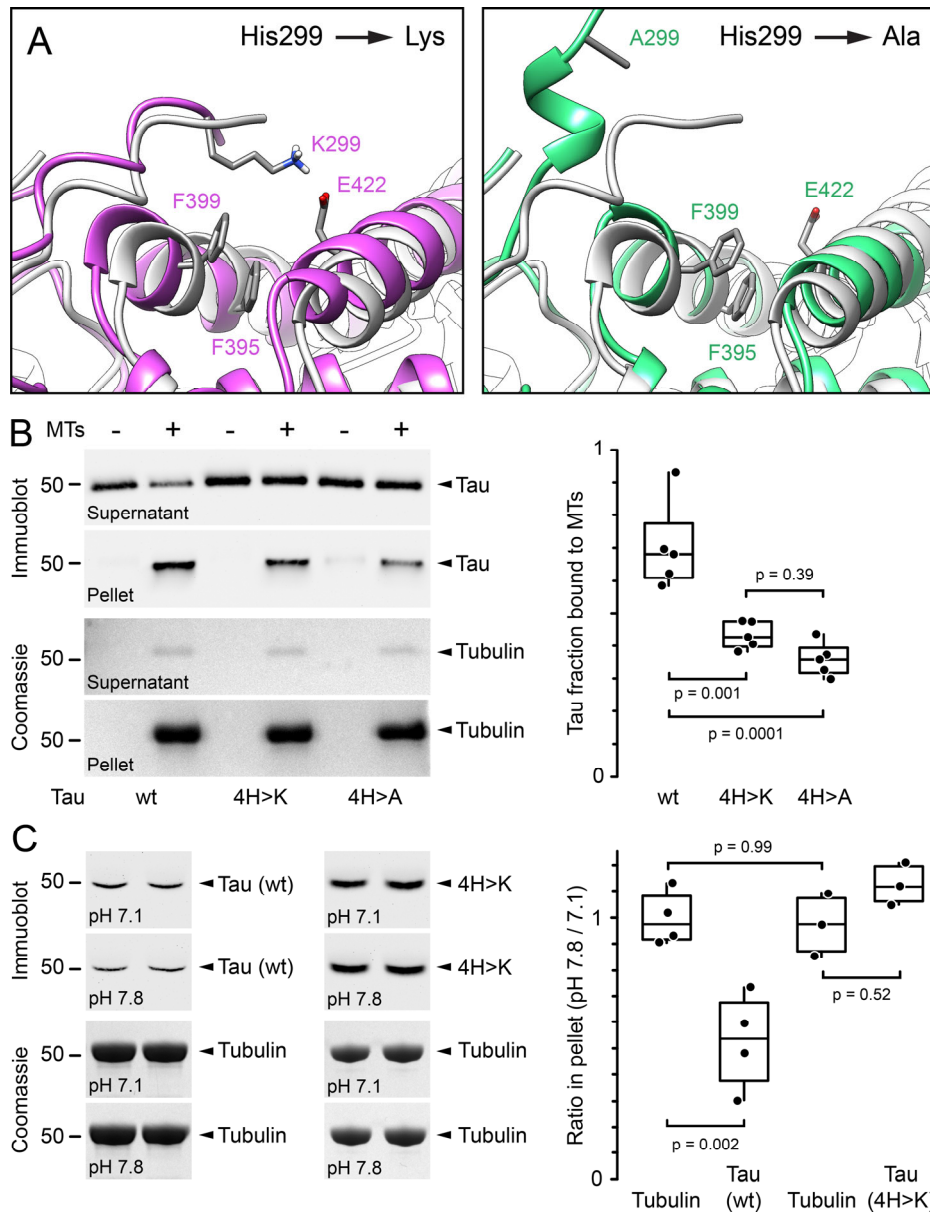
Figure 6. Conserved histidine residues modulate pH-dependent tau binding to MTs. (A) Close-up views of 5 ns MD simulations in which tau R2 His299 was substituted with either lysine or alanine as indicated overlaid with the cryo-EM structure shown in grey. (B) Co-sedimentation assay of 100 nM 0N3R tau protein with the indicated substitutions of conserved histidine residues with 1 µM paclitaxel-stabilized MTs at pH 6.8. Shown are immunoblots for tau and Coomassie-stained gels for tubulin in the supernatant and pellet. Note that tau remains in the supernatant in the absence of MTs. The boxplot shows a quantification of the tau fraction recovered in the pellet ($n = 5$). (C) Co-sedimentation assay of 10 nM 0N3R tau protein or 10 nM tau(4H>K) with 1 µM paclitaxel-stabilized MTs. Because tau is too diluted to be accurately detected in the supernatant only pellets of two independent experiments for each tau construct at the indicated pH values are shown. Equivalent amounts of pellets from different experiments were run in adjacent lanes on the same gels to minimize experimental error. The boxplot shows the ratio of either tubulin or tau in the pellet at pH 7.8 compared with pH 7.1 (wt: $n = 4$; 4H>K: $n = 3$). Statistical analysis by Tukey-Kramer HSD test.
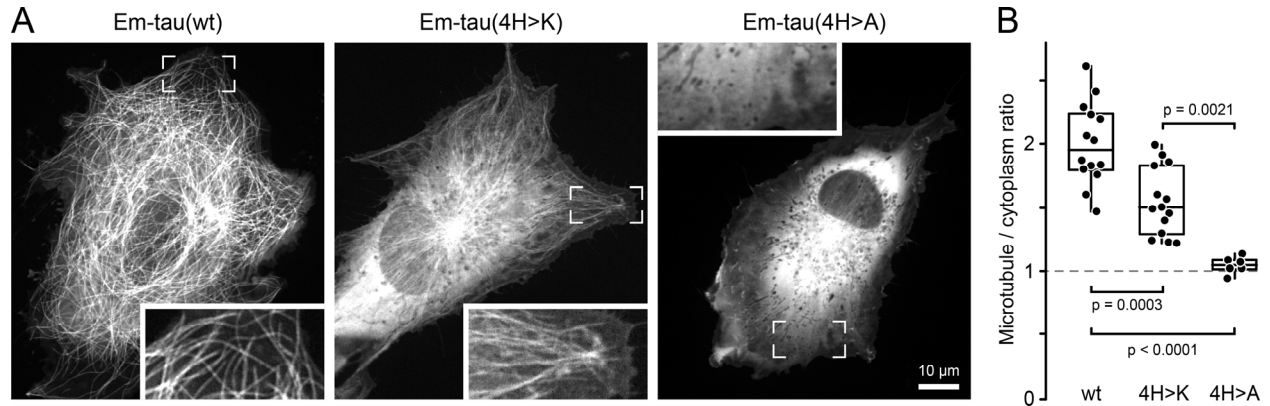
Figure 5. Conserved histidine residues are required for tau binding to MTs in cells. (A) RPE cells transiently expressing the indicated mEmerald-tagged tau constructs. Insets show highlighted regions at higher magnification. (B) Quantification of the relative enrichment of the indicated mEmerald-tau constructs on MTs compared to cytoplasm signal (wt and 4H>K: $n = 14$; 4H>A: $n = 6$ cells). The dashed line at a MT to cytoplasm ratio of one represents undetectable MT binding. Box plot shows median, first and third quartile, with whiskers extending to observations within 1.5 times the interquartile range, and all individual data points. Statistical analysis by Tukey-Kramer HSD test.